Experimental Investigation of Laminar Separation Bubbles and Comparison with Theory

E. Weibust,* A. Bertelrud,† and S.O. Ridder‡
FFA, The Aeronautical Research Institute of Sweden, Bromma, Sweden

Experimental and computational results from flow in and around laminar separation bubbles are given, with emphasis on the reattachment region. The experimental bubble parameters are correlated with existing formulas, utilizing a novel method of measuring with dense spacing in and behind the rear part of the bubble. Removal of the separation bubble by means of a transition trip is discussed.

Introduction

THE prediction of laminar separation bubbles creates numerous problems for aircraft design and development. The existence of laminar separation, bubble length, or failure to reattach, as well as implications concerning drag, have to be considered. Computational codes used, for example, in high-lift design[1,2] are critically dependent on the validity of empirical criteria.

This is an important issue also because a leading-edge stall for an airfoil may either be associated with a laminar bubble burst or, as pointed out by van den Berg,[3] be a turbulent separation. At low Reynolds number model tests the laminar bubble burst may take place, whereas the stall in flight may occur because of turbulent boundary-layer separation.

Despite considerable efforts, the engineering formulas used to predict the characteristics of laminar separation bubbles are unreliable even for two-dimensional flows. The physical modeling and description of the bubble structure is rather vague.

This is to some extent a consequence of the small physical dimensions of bubbles. The total height is often a fraction of a millimeter with bubble lengths of a few millimeters.

Any probing of the bubble with, for example, hot wires or pitot probes, may seriously affect the entire flowfield. As the bubble is located close to the leading edge of the airfoil, very few pressure taps can be located in the bubble region, and generally it is difficult to obtain data of sufficient quantity and quality to improve the mathematical description of short, laminar bubbles. Furthermore, most engineering criteria use the momentum thickness θ_s at laminar separation (i.e., the very start of the bubble) as scaling length, and computed values are often employed as reliable experimental values are very difficult to obtain.

A number of theories and criteria suitable for engineering predictions are available, as exemplified by Refs. 4–7. Distinction is made between long and short bubbles, and whether the bubble is close to or far from bursting. The bubble itself is split into a laminar part associated with the laminar shear layer from laminar separation back to transition and a turbulent part where the turbulent layer reattaches.

In the present paper, experimental results are given from the first phase in an investigation aimed at improving the reliability of engineering methods first in two dimensions and thereafter on a swept infinite wing. Over the past years more elaborate computational codes based on finitie difference schemes have been proposed for bubble prediction, but these have not been examined in the present stage of the project.

A more complete presentation of results can be found in Ref. 8.

Experiment

A modern airfoil[9] at negative angles of incidence was chosen for the experiment. Figure 1 shows the airfoil mounted in the L1 low-speed wind tunnel at the Royal Institute of Technology, Stockholm, Sweden. The tunnel speed could be varied continuously, and the airfoil was rotated through various angles of attack. Data acquisition was performed using an Apple II+ with an ISAAC data acquisition system for the time-averaged signals, and a.c. signals from two pressure transducers with high-frequency response, and six 1.5-mm/5-μm hot wires mounted in a miniature rake were recorded on a 14-track analog tape recorder.

The airfoil chosen for the experiment had a considerable straight region on the lower surface, i.e. the pressure side, allowing simplified installation of instrumentation. Figure 2 shows the airfoil and the definition of angle of attack used here. During the main part of the investigation a flap was mounted at an angle $\delta_F = 33.5$ deg to avoid stall due to trailing-edge separation, i.e., the stall should always be due to leading-edge bubble burst.

With normal spacing of static pressure taps, it may be a difficult task to identify various parts of the bubble, and it was considered crucial to the experiment that a sufficiently large number of experimental values could be obtained over and in the vicinity of the bubble.

Making the observation that the location of the separation point is rather insensitive to angle of attack,[7] a partly novel measurement technique was applied. Figure 3 shows how a part of the leading edge containing instrumentation appears to work properly as long as the boundary-layer rake is downstream of reattachment.

Instrumentation

1) Two fast pressure transducers (Kulite) were mounted 5 mm apart in the chordwise direction on a 0.05-mm-thick sliding metal ribbon, as indicated in Fig. 3. The ribbon was sliding on the airfoil and the transducers and cables run in a dig-out under the ribbon. Considerable care was taken to ensure that the ribbon was not deformed close to the pressure taps. The ribbon was movable by means of an electric motor

Presented as Paper 84-2201 at the AIAA 2nd Applied Aerodynamics Conference, Seattle, WA, Aug. 21-23, 1984; received March 14, 1985; revision received Oct. 1, 1986.

*Scientist.
†Senior Scientist, Head, Viscous Group. Member AIAA.
‡Senior Scientist.

inside the airfoil, and measurements could be obtained continously from −5 (i.e., below apex) to 180 mm (above apex).

2) To verify that the ribbon taps yielded valid results, a chordwise row of fixed pressure taps was located 50 mm from the ribbon. All static pressure taps, as well as the two located on the ribbon itself, had a diameter of 0.3 mm.

3) A pressure rake with eight 0.6-mm tubes was mounted on the ribbon behind the static pressure taps (Fig. 4a).

4) A hot-wire rake was also mounted on the ribbon at the same position as the pressure rake (Fig. 4b).

5) A 0.3-mm-diam Preston tube was mounted on the ribbon to obtain a measure of local skin friction. (Results are given in Ref. 8.)

The measurements were performed in three modes, depending on ribbon movement.

1) Ribbon moving back. Normal operation.

2) Ribbon moving forward. This was done to detect hysteresis.

3) Ribbon fixed. Discrete measurement points were obtained to make sure that ribbon movement could not bias results.

Results

Pressure Distributions

For practical reasons, mainly discrete measurement points are dealt with in the present paper, and only a few examples of the continuous pressure distributions are given.

Pressure distributions are presented both as normal C_p and canonical C_p; i.e., scaled by bubble pressure coefficient C_{p_B}:

$$\left[\frac{v}{v_B}\right]^2 = \frac{1-C_p}{1-C_{p_B}} \text{ (low subsonic)}$$

Figure 5 shows relatively long bubbles obtained at low α and low *Re*. The canonical pressure distributions indicate a total length of 25–30 mm, but a shift of bubble position with angle of attack.

The pressure distributions shown in Fig. 6 again confirm a bubble length almost independent of α, but the bubbles are, as could be expected at this somewhat higher Reynolds number, substantially shorter.

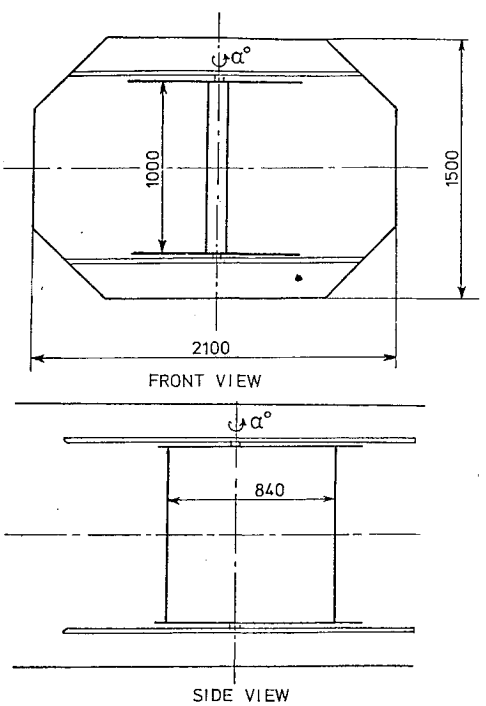

Fig. 1 Sketch of the model in wind-tunnel test section.

Both Figs. 5 and 6 reveal separation bubbles with approximately constant pressure under the laminar part of the bubble. This is in contrast to some measurements in literature, and this is analyzed further in Ref. 8.

Figure 7 shows pressure distributions at a yet higher Reynolds number. The trends are similar concerning bubble length and position, but here a pressure gradient is evident in the "plateau" part of the bubble.

The Reynolds number effect on the bubble at a low angle of attack, $\alpha = 3.5$ deg, is shown in Fig. 8. Here we note that the pressure distribution in the laminar acceleration region is independent of Reynolds number and, as expected, the value of C_p at the suction peak $C_{ps.p.}$ increases with Reynolds number. Note that the fluctuations in C_p values for the lowest *Re* are caused by low dynamic pressure and are mainly due to the resolution of digitized values. It should also be noted that the

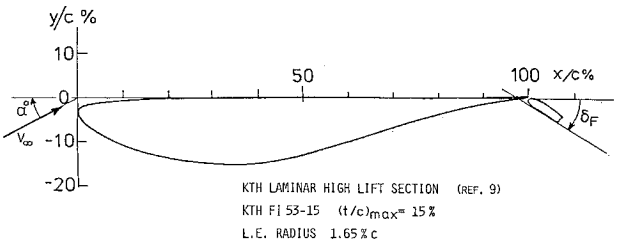

Fig. 2 Airfoil with position of fixed flap indicated.

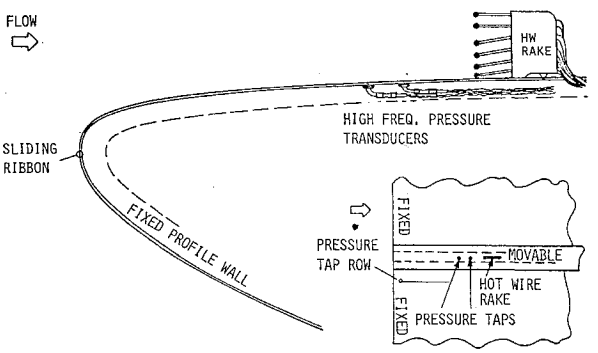

Fig. 3 Sketch of sliding skin (ribbon) and positions of static pressure taps and rakes.

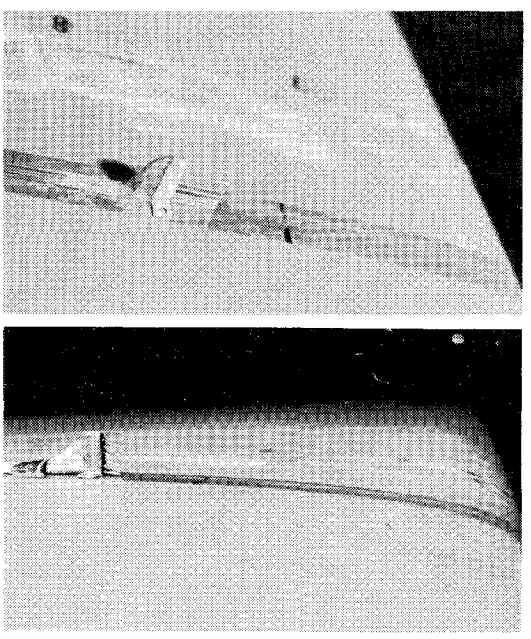

Fig. 4 a) Total head rake 20 mm aft of static pressure hole and b) HW rake attached to ribbon 20 mm aft of static pressure hole.

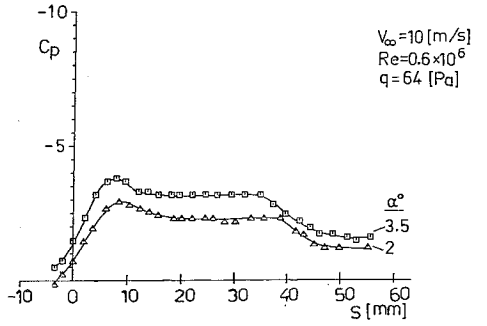

Fig. 5a Pressure distribution vs surface contour: $M=0.03$, $\delta_F=33.5$ deg.

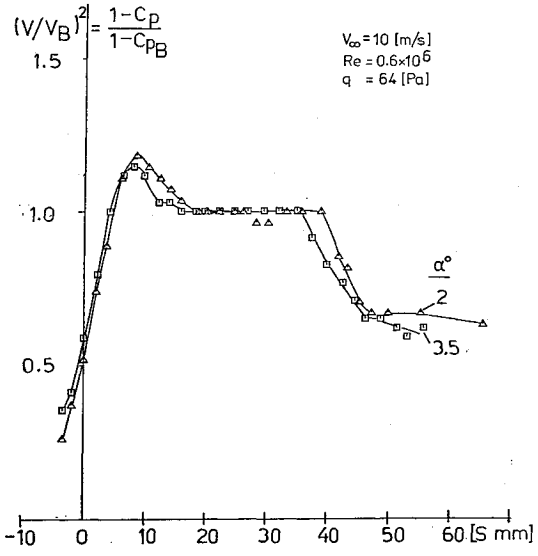

Fig. 5b Relative pressure distribution vs surface contour: $M=0.07$, $\delta_F=33.5$ deg.

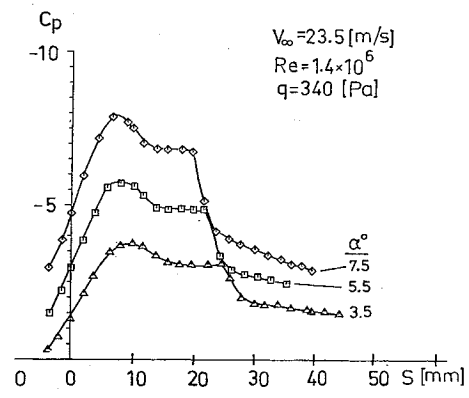

Fig. 6a Pressure distribution vs surface contour: $M=0.07$, $\delta_F=33.5$ deg.

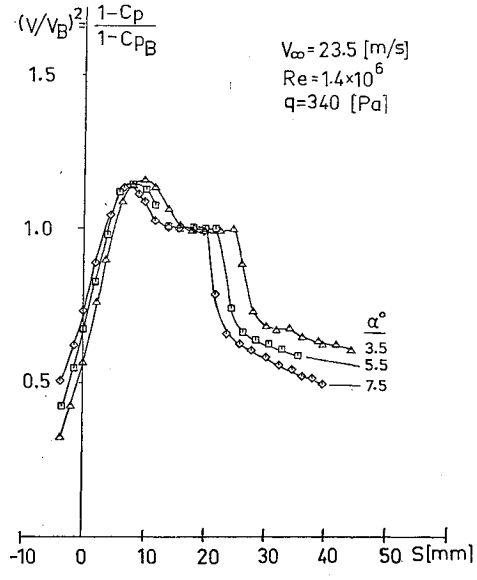

Fig. 6b Relative pressure distribution vs surface contour: $M=0.11$, $\delta_F=33.5$ deg.

$Re=0.4\times10^6$ case is very close to stall, and some of the scatter is probably due to unsteadiness.

Figure 9 shows the pressure distributions near maximum leading-edge suction, i.e., $(\alpha-\alpha_{stall})<0.5$ deg and illustrates the effect of Reynolds number in this case. The effect is particularly clear in the canonical pressure distribution, Fig. 9b.

While Figs. 5–9 show various features of the pressure distributions for a large variation in angle of attack as well as Reynolds number, the corresponding parametric variations as well as comparisons with theory will be dealt with in the next section.

Figure 10 may serve as a demonstration that the flow is really two-dimensional or at least has very small changes in the spanwise direction. Here the continuous pressure distributions obtained from the movable ribbon agrees extremely well with the results from the row of fixed pressure taps, even within the bubble itself.

Some runs were performed with a 0.1-mm-diam wire located 1 mm above the surface just at the position of the suction peak. The $C_{p\,s.p.}$ is increased considerably and, as is clear in Fig. 11, the laminar separation bubble has disappeared completely. Experiments performed with a thinner wire indicated a smaller "excess peak," and the thinnest wire used did not produce any noticeable peaks whereas it still removed the bubble.

It should be noted, however, that the angle of attack is very low and the bubble is not loaded for the case presented here. The pressure distribution far downstream of the bubble position has not been altered.

Another feature evident in Fig. 11 is the local increase in C_p value toward the rear of the bubble. At the reattachment there is a "dip" below the no-bubble case.

Boundary Layers

As mentioned earlier, it was important to avoid disturbing the flow, and in the present paper only boundary-layer data obtained behind the bubble is included.

Close behind reattachment rather high shape factors are obtained. The results for $\alpha=3.5$ deg in Fig. 12 indicate $H\simeq2$ decreasing to $H=1.6$ after a few centimeters. With Re_θ in excess of 1000, the turbulent layer is well established.

The boundary-layer development downstream of reattachment can be computed reasonably well. As is illustrated in Fig. 13, it is difficult to obtain accurate profile measurements in the thin turbulent layer, but use of Thompson profiles[10] in a computer-based form[11] gives a valuable way of interpreting the experiments. It also gives values for the skin friction that can be compared with the computations. The bubble's vertical size in the figure is small, and a rapid growth in boundary-layer thickness is evident. Note the relatively high velocities close to the wall.

One of the main questions concerning laminar separation bubbles is the drag penalty due to their presence. While measurements downstream of the bubble are difficult, proper measurements in the region right in front of the bubble are ex-

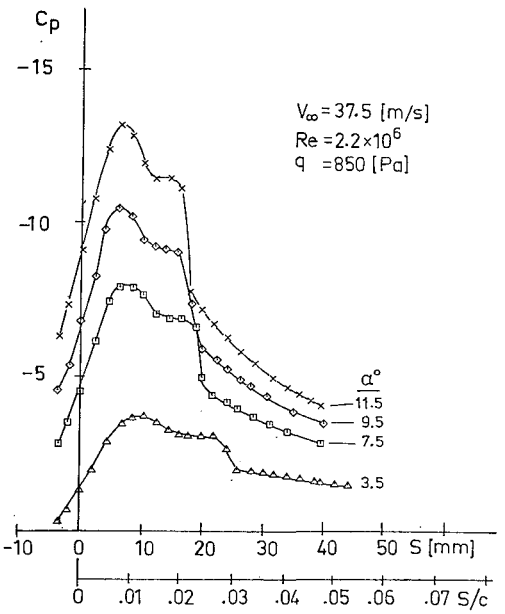

Fig. 7a Pressure distribution vs surface contour: $M = 0.11$, $\delta_F = 33.5$ deg.

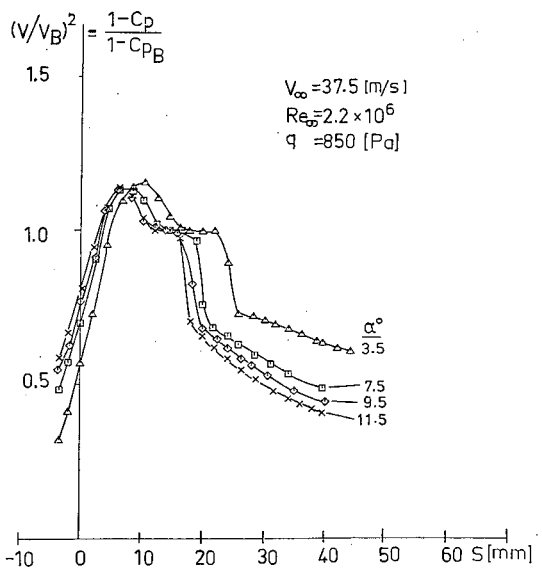

Fig. 7b Relative pressure distribution vs surface contour: $M = 0.11$, $\delta_F = 33.5$ deg.

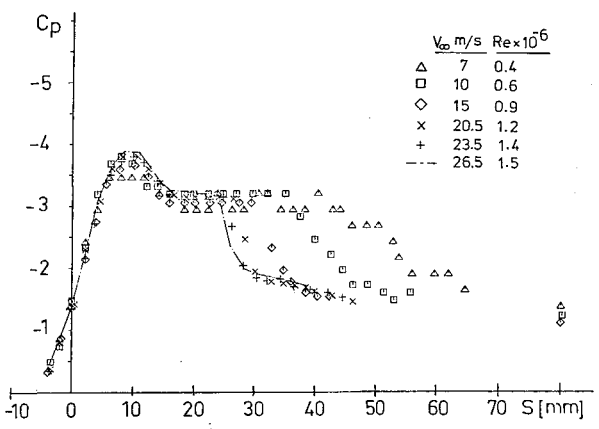

Fig. 8 Pressure distribution vs surface contour. Effects of *Re* at constant α: $\alpha = 3.5$ deg, $\delta_F = 33.5$ deg.

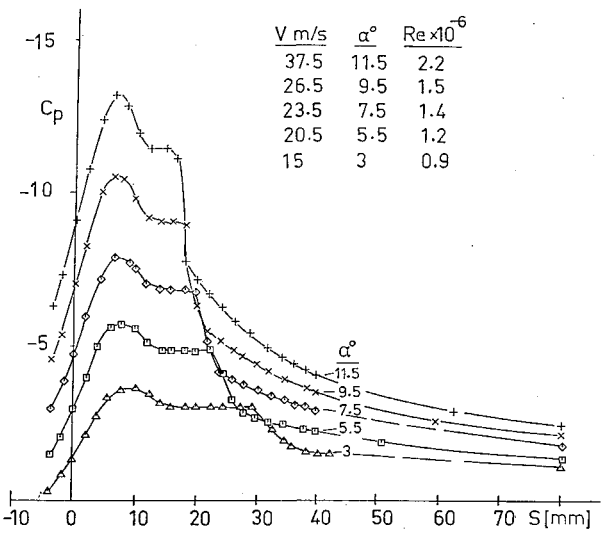

Fig. 9a Pressure distribution vs surface contour. Effects of *Re* at near maximum leading edge suction.

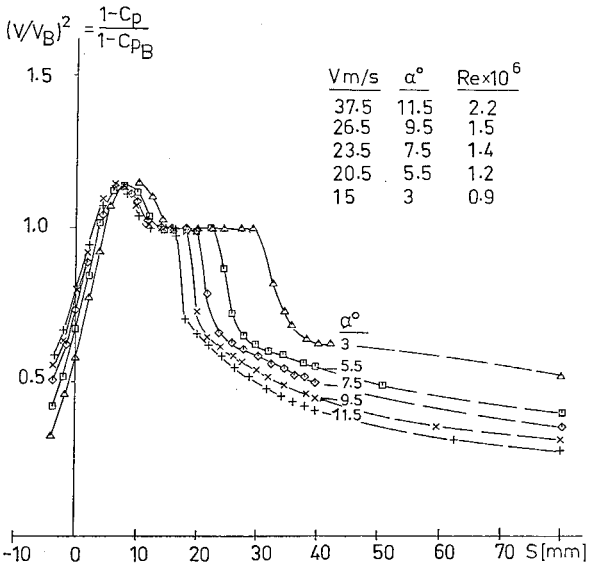

Fig. 9b Relative pressure distribution vs surface contour. Effects of *Re* at near maximum leading edge suction.

tremely difficult. Hence, the bubble drag penalty is normally estimated in the following manner:

1) Laminar boundary-layer calculation (integral method) from the stagnation point to the separation point. This is a common approach, but both in this context and in the comparisons with various formulas where θ_s is used as a scaling parameter, one should bear in mind that its value is very uncertain. The momentum thickness grows fast as separation is approached, and at the separation point itself the boundary-layer approximation is no longer valid.

2) Turbulent boundary-layer calculation (integral method) using an assumed, smooth pressure distribution back to the region where the experimental boundary-layer profiles are related. The difference between the experimental and the computed θ now yields the drag penalty due to the bubble. In the present cases, this may cause some problems, as the computed Re_{θ_s} values actually in many cases yield the s very existence of a turbulent boundary layer as unrealistic.

In Ref. 8, the computed boundary-layer development is exemplified for different Reynolds numbers, and the drag penalty of the bubbles is indicated in terms of an amplification factor.

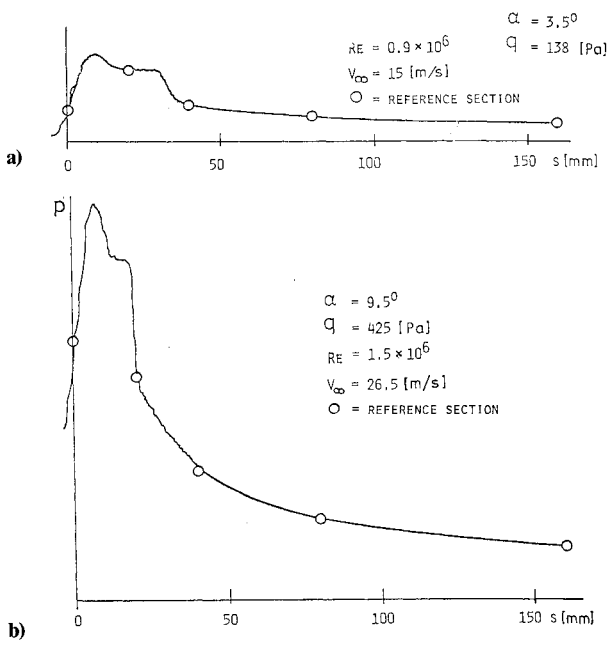

Fig. 10 Pressure distribution (analog signal), comparison with reference section.

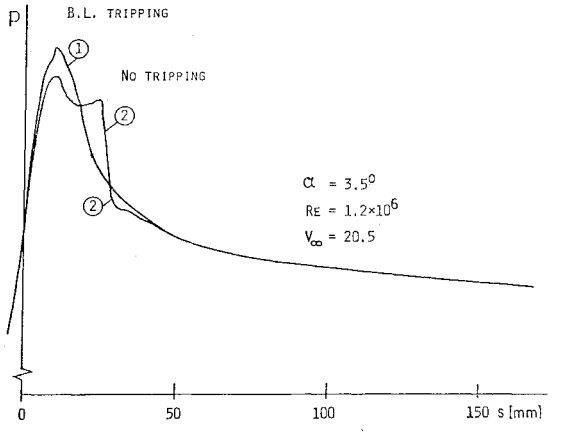

Fig. 11 Effect of boundary-layer tripping on static pressure distribution (analog signal). Metal string, $\phi = 0.1$ mm, 1 mm above surface just at position of suction peak.

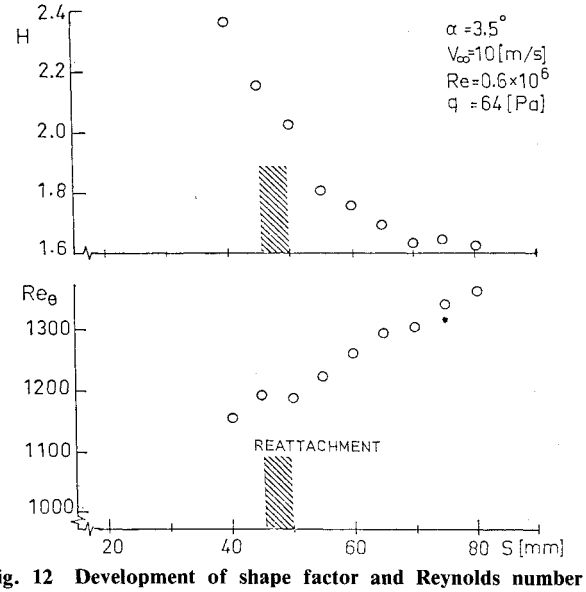

Fig. 12 Development of shape factor and Reynolds number (as determined from total head rake) in the reattachment region and downstream.

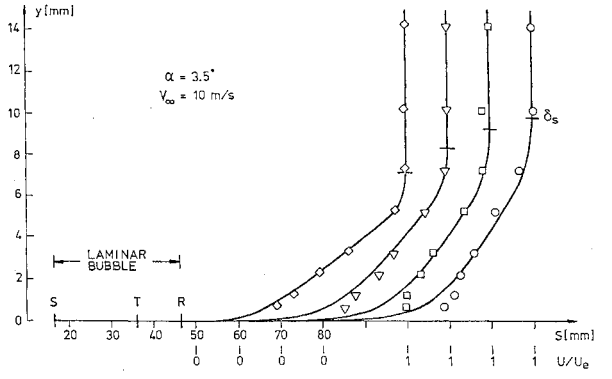

Fig. 13 Velocity profiles downstream of reattachment. Open symbols are experimental results, lines are corresponding Thompson profiles.

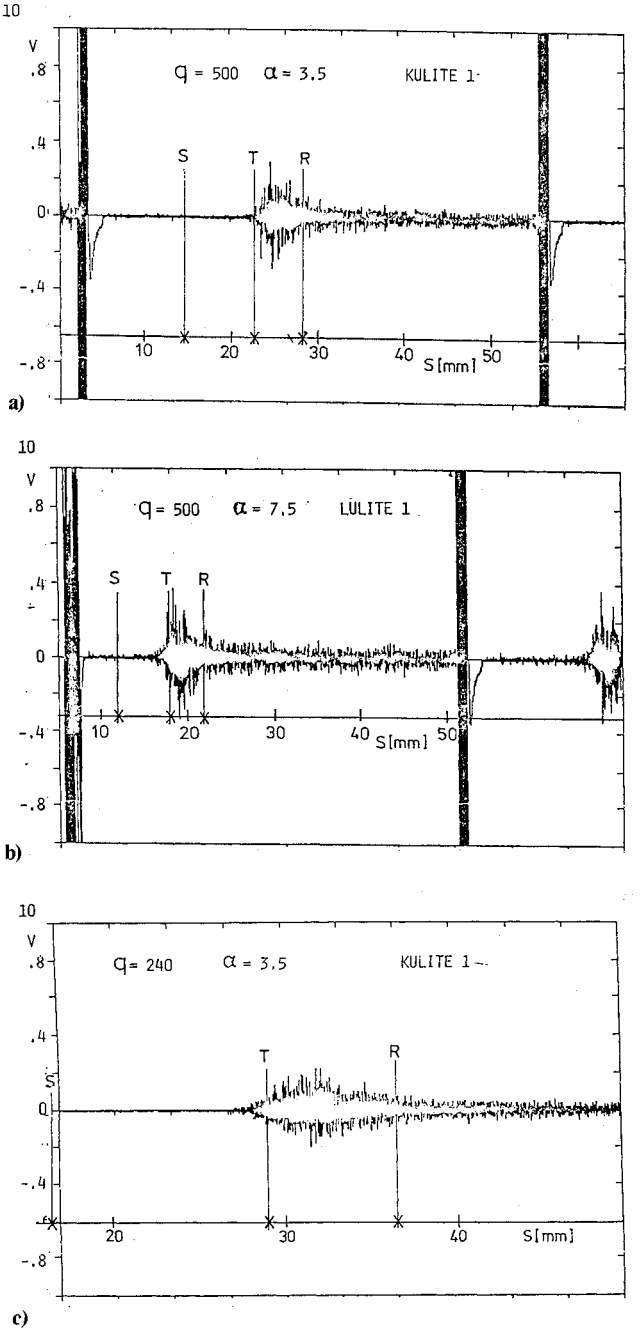

Fig. 14 Static pressure fluctuations in front of, inside, and behind laminar separation bubbles. S-T-R indicate bubble positions as determined from the time-averaged static pressure distributions.

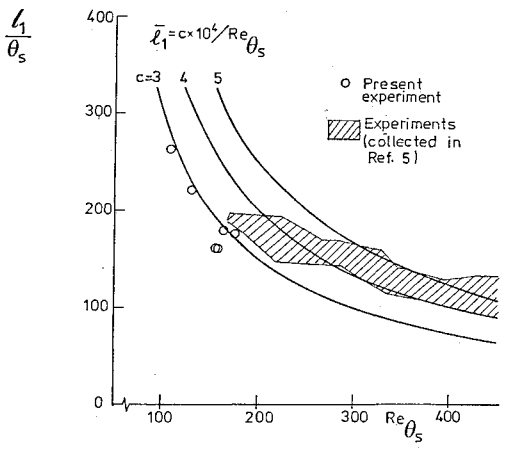

Fig. 15 Length of the laminar part of the separation bubble.

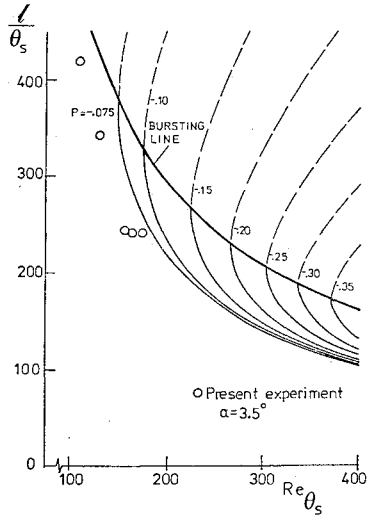

Fig. 16 Total bubble length $\bar{\ell}$ vs Re_{θ_s}. The dashed curves are physically unrealistic conditions. Computations are from Ref. 5.

The local skin-friction development is discussed in Ref. 8. A variety of measurement techniques exist, but most of them are not feasible to use in the present thin, high-pressure-gradient boundary layer.

The technique chosen was a Preston tube with extremely small diameter (0.3 mm) mounted on the moving ribbon 15 mm behind a static pressure tap. By monitoring the total pressure of the tube, the bubble and reattachment could be identified.

Pressure Fluctuations

A number of recordings were made with the fast pressure transducers either at various fixed positions inside or in the vicinity of the bubble, or slowly moving through the bubble.

Figure 14 shows three typical recordings obtained at various conditions. The letters S, T, and R correspond to the positions of laminar separation, transition, and reattachment, respectively.

As can be seen, there are almost no fluctuations in front of separation or beneath the free shear layer in front of transition. As transition has been estimated from the change in time-averaged static pressure, the latter part of the constant pressure region demonstrates fluctuations growing rapidly in amplitude. In the pressure-rise region, the fluctuations are largest, but with no particular feature at the reattachment position itself. The turbulent relaxing layer downstream exhibits a fair amount of fluctuations. When comparing the

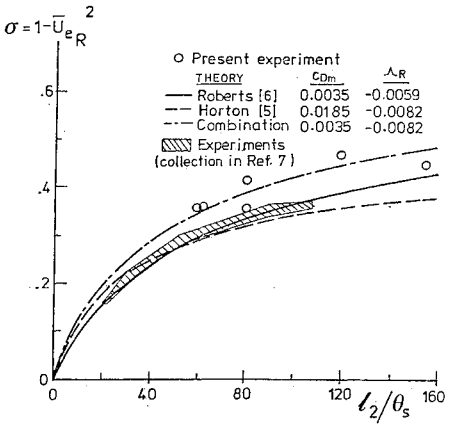

Fig. 17 Nondimensional velocity loss vs length of turbulent bubble region.

three different cases, the absolute value of pressure fluctuations appears to be roughly the same, irrespective of dynamic pressure or angle of attack, and the main effect to observe is that the extent of the various regions simply follows the length scale of the bubbles.

Computations

In this section, some comparisons are made with the theory and experimental data presented by Horton[5] and Roberts.[6]

The bubble length is predicted according to

$$\bar{\ell}_1 = \frac{\ell_1}{\theta_s} = \frac{4 \times 10^4}{Re_{\theta_s}} \quad \text{(laminar part)}$$

$$\bar{\ell}_2 = \frac{\ell_2}{\theta_s} = \frac{B_1(1 - \bar{U}_{e_R})}{\bar{U}_{e_R}^4 - C_1} \quad \text{(turbulent part)}$$

where

B_1 = $1/((C_{dm}/4H_{\epsilon m}) - \Lambda_R)$; $C_1 = (C_{dm}/4H_{\epsilon_\omega})B_1$
Re_{θ_s} = Reynolds number based on θ at separation
C_{dm} = mean dissipation coefficient, = 0.035
$H_{\epsilon m}$ = boundary-layer parameter based on energy thickness ϵ, = 1.5
Λ_R = reattachment criterion, $\theta/U_e \cdot (dU_e/ds)$
$\bar{U}_{e_R}$ = U_{e_R}/U_{e_s}

As Fig 15 inidicates, the expression for $\bar{\ell}_1$ appears as a reasonable approximation—especially at the low Reynolds numbers encountered here.

It may be observed that C here is merely the Reynolds number based on local velocity and length from the separation point, i.e., it is not dependent upon any assumed θ_s value. Roberts[6] has suggested using a criterion based on the freestream turbulence intensity and length scale. At present, this information has not been evaluated properly.

Figure 16 may be used to illustrate closeness to bubble burst for the experimental cases at $\alpha = 3.5$ deg. The parameter P is given by

$$P = \frac{\theta_s^2}{\nu} \frac{\Delta U}{\Delta X}$$

and

$$\bar{\ell} = \frac{\ell_1 + \ell_2}{\theta_s}$$

is the total bubble length and $\Delta U/\Delta x$ is the velocity gradient over the bubble.

Figure 17 shows the relation between the length of the turbulent, reattaching shear layer and the velocity ratio over the bubble; here given as Crabtree's parameter σ. The σ values of the present experiment are high, but it is interesting to see that the differences obtained using various constants in the theory yield a quite large span in the correlation.

Conclusions

From the present exploratory study the following conclusions may be drawn:

1) Use of a thin, movable ribbon with static pressure taps is very valuable to obtain detailed pressure data for evaluation of bubble criteria.

2) It is possible, even at low Reynolds numbers, to remove the bubble using a localized disturbance close to the suction peak. The resulting pressure distributions correspond to a much higher simulated Reynolds number.

3) The static pressure fluctuations grow very rapidly at the rear of the laminar free shear layer.

4) Thompson profiles are convenient for use even close behind turbulent reattachment.

5) The findings of Horton[5] and Roberts[6] are generally confirmed.

A more comprehensive collection of data can be found in Ref. 8. The immediate plans concern more complete measurements at selected angles of attack and Reynolds numbers.

Acknowledgments

This work is sponsored by the National Swedish Board for Technical Development within the Research Program for Civil Aircraft Technology. The assistance of I. Engström in preparing the manuscript is also gratefully acknowledged.

References

[1]Stevens, W.A., Goradia, S.H., and Braden, J.A., "Mathematical Model for Two-Dimensional Multi-component Airfoils in Viscous Flow," NASA CR-1843, 1971.

[2]Dvorak, F.A., Woodward, F.A., and Maskew, B., "A Three-Dimensional Viscous/Potential Flow Interaction Analysis Method for Multi-Element Wings," NASA CR-152012, 1977.

[3]van den Berg, B., "On the Role of Laminar Separation Bubbles in Airfoil Leading Edge Stall," National Lucht-ess Ruimtwaart-laboratorium, The Netherlands, NLR Rept. MP 80010U, 1980.

[4]Stratford, B.S., "Flow in the Laminar Boundary Layer Near Separation," ARC R&M 3002, 1957.

[5]Horton, H.P., "A Semi-Empirical Theory for the Growth and Bursting of Laminar Separation Bubbles," ARC CP 1073, 1969.

[6]Roberts, W.B., "Calculation of Laminar Separation Bubbles," AIAA Journal, Vol. 18, No. 1, 1980, pp.25-31

[7]van Ingen, J.L., "Theoretical and Experimental Investigations of Incompressible Laminar Boundary Layers with and without Suction," Technological University, Delft, Netherlands, Rept, VTH-124, 1965.

[8]Weibust, E., Bertelrud, A., and Ridder, S.O., "Laminar Separation Bubbles—An Exploratory Study," FFA TN 1984-61, 1987.

[9]Ridder, S.O., "Wind Tunnel Tests of a 15% Thick Laminar Wing Section with a 25% Chord Trailing Edge Flap," KTH AERO, Stockholm, Sweden, Rept. FI 53, 1980.

[10]Thompson, B.G.J., "A New Two-Parameter Family of Mean Velocity Profiles for Incompressible Turbulent Boundary Layers on Smooth Walls," ARC R&M 3463, 1967.

[11]Bertelrud, A., "Computer-Generated Thompson Profiles," FFA TN 1984-60, 1987.